SCIENTIFIC REPORTS

OPEN

SUBJECT AREAS:
PHOTOCATALYSIS
HETEROGENEOUS CATALYSIS
PHOTOCHEMISTRY
CHEMICAL ENGINEERING

Received
29 October 2013

Accepted
23 December 2013

Published
22 January 2014

Correspondence and requests for materials should be addressed to X.B.K. (x.ke@qut.edu.au)

Plasmonic nanostructures to enhance catalytic performance of zeolites under visible light

Xingguang Zhang, Xuebin Ke, Aijun Du & Huaiyong Zhu

School of Chemistry, Physics and Mechanical Engineering, Queensland University of Technology, QLD 4001, Australia.

Light absorption efficiency of heterogeneous catalysts has restricted their photocatalytic capability for commercially important organic synthesis. Here, we report a way of harvesting visible light efficiently to boost zeolite catalysis by means of plasmonic gold nanoparticles (Au-NPs) supported on zeolites. Zeolites possess strong Brønsted acids and polarized electric fields created by extra-framework cations. The polarized electric fields can be further intensified by the electric near-field enhancement of Au-NPs, which results from the localized surface plasmon resonance (LSPR) upon visible light irradiation. The acetalization reaction was selected as a showcase performed on MZSM-5 and Au/MZSM-5 ($M = H^+$, Na^+, Ca^{2+}, or La^{3+}). The density functional theory (DFT) calculations confirmed that the intensified polarized electric fields played a critical role in stretching the C=O bond of the reactants of benzaldehyde to enlarge their molecular polarities, thus allowing reactants to be activated more efficiently by catalytic centers so as to boost the reaction rates. This discovery should evoke intensive research interest on plasmonic metals and diverse zeolites with an aim to take advantage of sunlight for plasmonic devices, molecular electronics, energy storage, and catalysis.

Photocatalysis has significantly advanced in developing efficient catalysts to harvest the "green" solar energy at ambient conditions. Recent years have seen a new family of plasmonic photocatalysts of gold, silver, or copper nanoparticles (NPs), which features a collective and coherent oscillation of the free conduction electrons with the incident photons at the surface of NPs due to the localized surface plasmon resonance (LSPR) irradiated by visible light[1–3]. This LSPR effect has been applied to boost catalytic performance in various important organic transformations under the irradiation of visible light: oxidation of organic contaminants and aromatic alcohols, and reduction of nitroaromatic compounds, ketones and epoxides on Au-NPs[4–7]; epoxidation of ethylene on Ag-NPs and of propylene on Cu-NPs[8,9]. Very recently, Au-Pd alloys are also founded to be efficient photocatalysts for Suzuki coupling reactions and oxidation of benzylamine[10,11]. These discoveries demonstrate that the plasmon-mediated processes fundamentally differ in catalytic mechanisms compared with those on traditional semiconductors. Moreover, the LSPR effect of plasmonic NPs can amplify the electromagnetic field intensity of incident light ($|E_0|$) and results in an enhanced electric field ($|E|$) of 3–6 orders of magnitude[3,12]. This near-field enhanced interaction is well-known as the "electric near-field enhancement (ENFE)" effect and has motivated numerous intensive studies, such as surface-enhanced Raman scattering[13], sensors[14–16], plasmonic devices[17–19] and solar cells[20,21]. In photocatalysis, Ag-NPs covered by the SiO_2 shell and embedded in TiO_2 particles have been tried to degrade methyl blue and exhibit better catalytic performance owing to the electric field amplitude effect of Ag-NPs[22]. However, the inert SiO_2 shell, which is used to prevent the Ag core from oxidation, constraints the light absorption efficiency in photocatalysis.

Zeolites possess regular microporous structures, high surface areas, shape-selectivity, and unique solid acidity, having extensive applications in catalysis, separation, and adsorption. Particularly, the strong polarized electrostatic fields (PEF, 1–10 V/nm) created by extra-framework cations have the power to polarize molecules adsorbed on surfaces or confined in the porous matrix (e.g. host-guest structures)[23–25]. In principle, the PEF can reduce the energy consumption required to facilitate the electron transfer or to activate reactants, thereby initiating reactions by moderate heating or visible-light excitation. The charge-transfer properties from hydrocarbons to molecular oxygen (O_2) have been investigated on ion-exchanged zeolites, such as ZSM-5, Y and Beta, with visible light irradiation in the selective oxidization of toluene, propane, cyclohexane, and small alkenes[26–29]. These studies verify that the PEF can lower the charge-transfer excitation energy from hydrocarbons to O_2. However, the

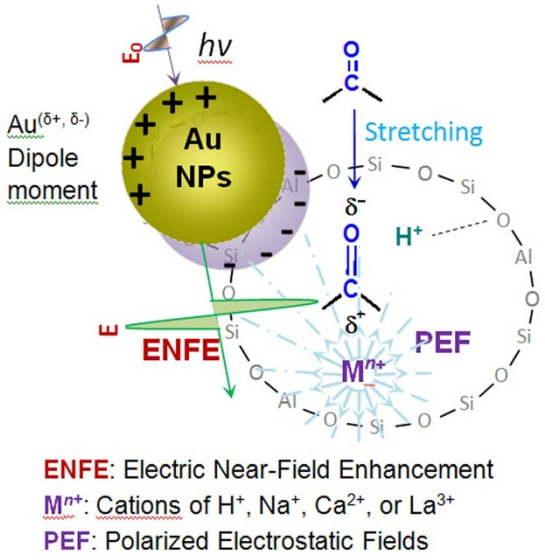

Figure 1 | The acetalization on Au/MZSM-5 (M = H^+, Na^+, Ca^{2+}, or La^{3+}) under the irradiation of visible light. ENFE means the electric near-field enhancement of Au-NPs. PEF means the polarized electro-static fields of extra-framework cations in zeolites.

products cannot be quantitatively measured because of low productivity, which results from the low absorption efficiency of zeolites of visible light.

Plasmonic Au-NPs are loaded on ion-exchanged ZSM-5 zeolites (Au/MZSM-5, M = H^+, Na^+, Ca^{2+}, or La^{3+}) as "antenna" to efficiently absorb visible light. This study for the first time reports a cascade enhancement from visible light to zeolites via the LSPR-induced ENFE which functions as a "relay" to intensify the PEF of cations in zeolites to boost the catalytic performance. The acetalization of benzaldehyde with 1-pentanol is selected as the model reaction[30–34]. The present research demonstrated that the ENFE of Au-NPs could intensify the PEF of MZSM-5 so as to facilitate the effective activation of the reactant of benzaldehyde by stretching the C=O bonds, thus improving the conversion of the acetalization.

To illustrate this enhancing process, as shown in Figure 1, Au-NPs form dynamic $Au^{(\delta+,\ \delta-)}$ dipole moments owing to the LSPR effect upon visible light irradiation, simultaneously inducing the ENFE around the surface of Au-NPs[2,3]. The ENFE intensifies the PEF of extra-framework cations in MZSM-5, which enables the intensified PEF to stretch the C=O bond of reactants of benzaldehyde. The stretched reactants display larger molecular polarities and can be activated more efficiently by catalytic active centers of H^+, thereby accelerating reactions with alcohols[35]. The Brønsted acid sites originate from terminal hydroxyl groups, and extra-framework cations: $M^{2+} + H_2O + \text{Si-O-Al} \rightarrow M(OH)^+ + \text{Si-O}(H^+)\text{-Al}$[24,36].

Table 1 revealed that the acetalization between benzaldehyde and 1-pentanol proceeded effectively on Au/MZSM-5 under visible light irradiation. The catalytic conversions improved significantly on Au/NaZSM-5, Au/CaZSM-5, and Au/LaZSM-5; particularly, the conversion increased from 21.5% on CaZSM-5 to 62.2% on Au/CaZSM-5 (an exception for HZSM-5 will be interpreted later). However, with light off (see SI, Table S1, Section S1), the catalytic conversions of MZSM-5 and Au/MZSM-5 showed fewer differences, indicating Au-NPs themselves were not active centers under dark conditions. Moreover, visible light irradiation showed negligible influence on the activity of MZSM-5 compared with those under dark conditions. These results confirmed that visible light and plasmonic Au-NPs were necessities to sharply boost the acetalization reaction.

The differences in conversions on MZSM-5 indicated that extra-framework cations markedly influenced the catalytic activity. HZSM-5 exhibited the highest conversion of 53.8%, whereas NaZSM-5, CaZSM-5, and LaZSM-5 exhibited lower conversions (just better than Silicalite-1) primarily because of their relatively fewer active centers (H^+). The change in Brønsted acidity could be proved by the spectra of FT-IR spectroscopy - attenuated total reflectance (ATR) which also confirmed that Brønsted acids preserved well after loading of gold (see SI, Figure. S1, Section S2).

Moreover, the optical properties of catalysts were investigated by UV/Vis spectra (Figure 2a), showing that MZSM-5 had no measurable absorption of visible light (>420 nm), whereas Au/MZSM-5 strongly absorbed visible light owing to the LSPR effect of Au-NPs, with the absorption peaks being about 525–565 nm. The crystal structures of Au/MZSM-5 were detected by X-ray diffraction (XRD) patterns (Figure 2b), confirming that the MFI structures preserved well. The oxidation state of gold was analyzed by X-ray photoelectronic spectra (XPS) (Figure 2c) which identified that the binding energies of Au$4f_{7/2}$ electrons (84.1 eV) and Au$4f_{5/2}$ electrons (87.7 eV) were in agreement with reports for Au-NPs[37]. In addition, XPS showed that the gold content were similar on Au/MZSM-5, the Si/Al ratio was close to 14, and that the ion-exchange level was high because Na^+ ions were undetectable in CaZSM-5 and LaZSM-5. Transmission-electron-microscopy (TEM) images provided direct information of the size (6–18 nm), shape (pseudospherical) and distribution of Au-NPs on zeolites (see SI, Figure. S3, Section S3).

Now one may wonder why visible light coupled with Au-NPs could boost the reaction on Au/MZSM-5. Here we hypothesize that the ENFE of Au-NPs directly intensifies the PEF of cations to a large extent that the intensified PEF can polarize reactants of benzaldehyde and 1-pentanol to facilitate activation of them by catalytic active centers of H^+. From the experimental perspective, Au/HZSM-5 and HZSM-5 exhibited similar catalytic activities with light on, as shown in Table 1, indicating that Au-NPs neither served as extra active centers nor interacted directly with the reactants to accelerate the reaction rate even though the LSPR-induced dipole moment of $Au^{(\delta+,\ \delta-)}$ could in theory interact with the reactants. In this case, there should exist other key factors that affected the interaction with reactants. The density functional theory (DFT, see SI, Section S4) calculations unambiguously demonstrated that increasing the strength of external electric field stretched the C=O bond of benzaldehyde, whereas had no effect on 1-pentanol, probably because the molecular polarity of benzaldehyde (dipole moment $\mu = 3.00$ Debye) is larger than that of 1-pentanol (1.70 Debye). The relationship between the C=O bond length and the electric field strength was linear (Figure 3a). In detail, the C=O bond lengths of benzaldehyde were 1.218 Å, 1.223 Å, 1.229 Å, 1.236 Å, and 1.245 Å, when the electric field strengths were 0 V/nm, 2.58 V/nm, 5.16 V/nm, 7.74 V/nm, and 10.32 V/nm, respectively. Here the electric field strength used in simulation were on the same order of magnitude as that reported for HZSM-5 (3.0 V/nm), NaZSM-5 (6.2 V/nm), CaZSM-5 (8.3 V/nm), and LaZSM-5 (10.7 V/nm) (see SI, Table S2, Section S5)[23,38]. However, the experimental results revealed that the PEF of MZSM-5 without Au-NPs had no influence on the conversions, which indicated that the PEF of MZSM-5 was not strong enough to boost the reaction rate even with light on.

These results trigger a logical deduction that further increasing the electrostatic field strength may make distinct difference. And it has been underpinned by the experimental evidence that the existence of an external electric field of 12–15 V/nm obviously helps activate the reactants of CO/O_2 and enhances the oxidation process on small gold crystals (20–30 nm). This effect is considered to be associated with the formation of partially charged gold surface[39]. Furthermore, it has been reported that the near-field enhancement factor ($|E|/|E_0|$) of plasmonic NPs can reach as large as 10^2 at the surface of individual NPs and 10^3 at the junction of interparticles (hot spots)[40,41], and that the ENFE attenuates exponentially within the spacing range of 10–50 nanometers away from metal surfaces, depending on the metal

Table 1 | Catalytic performances of the acetalization between benzaldehyde and 1-pentanol on MZSM-5 and Au/MZSM-5 (M = H^+, Na^+, Ca^{2+}, or La^{3+}) under visible light irradiation

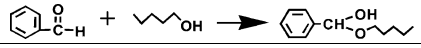

Catalyst	Conv.[a] (%)	Sele.[b] (%)	Yield (%)	Reaction rate (10^{-3} molg^{-1} h^{-1})
CaZSM-5	21.5	>99	21.3	4.37
Au/CaZSM-5	**62.2**	99.1	**61.6**	12.79
NaZSM-5	30.9	>99	31.6	6.28
Au/NaZSM-5	**52.5**	97.8	**51.3**	10.80
LaZSM-5	48.7	>99	48.2	9.90
Au/LaZSM-5	**58.4**	96.5	**56.4**	12.01
HZSM-5	53.8	>99	53.3	10.93
Au/HZSM-5	**55.8**	98.7	**55.1**	11.48
Silicalite-1	9.3	>99	9.2	1.91
Au/Silicalite-1	**11.5**	96.5	**11.1**	2.37

[a]: the conversion of benzaldehyde.
[b]: the selectivity towards pentyloxy(phenyl)methanol. Reaction conditions: benzaldehyde (0.65 g), 1-pentanol (4.40 g); temperature (60°C), time (6 h); light intensity (0.5 W/cm^2), wavelength range (420–800 nm); catalyst (0.05 g); atmosphere (air). No detectable reaction without catalysts.

crystal size and shape, and the dielectric environments[1]. Therefore, it becomes convincing that the ENFE may directly intensify the PEF of cations in MZSM-5 to a large extent so as to stretch the C=O bond of reactants, thereby boosting the reaction rate.

The intensified PEF of H^+, Na^+, Ca^{2+}, and La^{3+} differed in boosting the catalytic activities on Au/MZSM-5. The largest net increase in the conversion of acetalization reaction, which means the conversion on Au/MZSM-5 deducts the conversion on its counterpart of MZSM-5, occurred between Au/CaZSM-5 and CaZSM-5, and the lowest between Au/HZSM-5 and HZSM-5 (Figure 3b, calculated from Table 1). It has been reported that the PEF strength of a single cation within a given zeolite host is influenced by multi-factors, such as Si/Al ratio, charge/radius ratio, cation charges and cation density (see SI, Table S2, Section S5). As for Au/HZSM-5 and HZSM-5, the original PEF strength of H^+ is ca. 3.0 V/nm and the intensified PEF strength of H^+ might be still too weak to stretch the C=O bond of benzaldehyde, thus showing the lowest net increase in conversion. The intensified PEF strength of Na^+ (originally ca. 6.2 V/nm), Ca^{2+} (originally ca. 8.3 V/nm), or La^{3+} (originally ca. 10.7 V/nm) should be sufficiently strong to extend the C=O bond of benzaldehyde to accelerate the reaction. Interestingly, La^{3+} ions which had the strongest electrostatic field showed a lower net increase of conversion than Na^+ ions and Ca^{2+} ions. This phenomenon probably resulted from the difference in cation density within MZSM-5 after ion-exchange because one La^{3+} ion corresponds to three Na^+ in terms of compensating for the negatively-charged framework sites (see SI; Section S5, Table S3, and Section S6); therefore, the number of La^{3+} (La^{3+}/Al = 0.09) was smaller in MZSM-5 compared with the number of Na^+ (Na^+/Al = 0.43) or Ca^{2+} (Ca^{2+}/Al = 0.25), thereby exhibiting a lower net conversion between Au/LaZSM-5 and LaZSM-5. One may argue that the acidity of zeolites plays a more important role than PEF in the acetalization reaction because Brønsted acid sites (H^+) are the catalytic centers. However, this study conveys a clear message that the intensified PEF by ENFE does contribute to improving the catalytic performances of zeolites by affecting the molecular polarities of reactants.

The impacts of light intensity, the range of wavelength, and reaction temperature on the acetalization reaction were investigated on CaZSM-5 and Au/CaZSM-5 with light on. As shown in Figure 4a, the increase of light intensity improved the catalytic activity on Au/CaZSM-5, but not on CaZSM-5. This result indicated that raising the light intensity could afford a much stronger ENFE on Au/CaZSM-5 thus contributing more to boosting the catalytic activity. The light wavelength was also investigated using glass filters to block photons with wavelengths below the filter threshold. For example, the cut-off wavelength of 420 nm means that the light with wavelength smaller than 420 nm was blocked. Figure 4b showed that the light wavelength significantly influenced the catalytic activity of Au/CaZSM-5, but not on CaZSM-5. This result demonstrated a wavelength-selective enhancement on Au/CaZSM-5, and proved that visible light that could induce the ENFE effect of Au-NPs made a larger contribution to boost the catalytic activity. Raising the reaction temperature increased the conversions both on CaZSM-5 and Au/CaZSM-5 (Figure 4c). The conversion on Au/CaZSM-5 was much higher than that on CaZSM-5 at the same temperature. The slight decrease in selectivity could be ascribed to the oxidation of

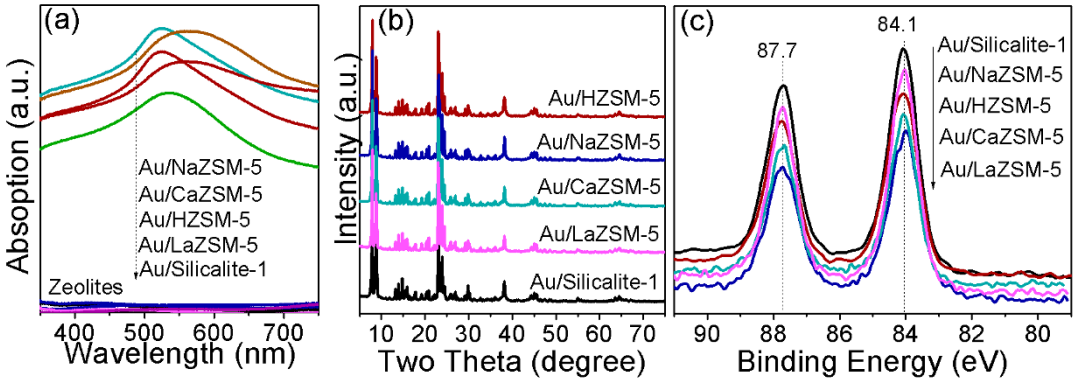

Figure 2 | Characterizations of Au/Silicalite-1 and Au/MZSM-5 (M = H^+, Na^+, Ca^{2+}, or La^{3+}): (a) UV/Vis spectra, (b) XRD patterns, and (c) XPS spectra.

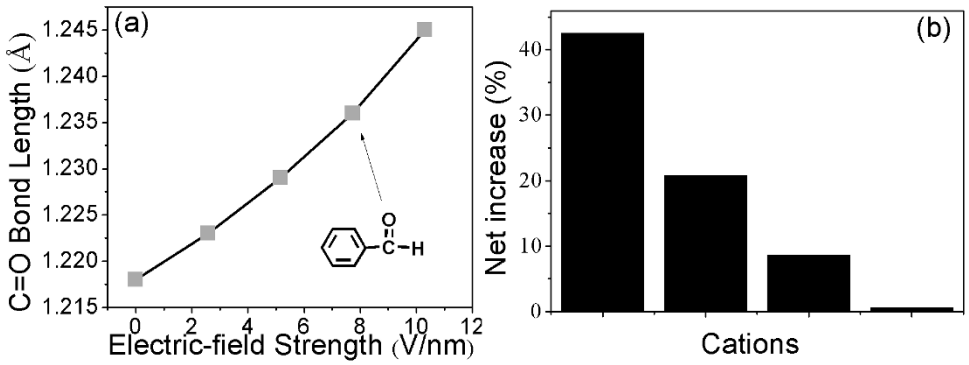

Figure 3 | (a) The relationship between the C=O bond length (Angstrom) of benzaldehyde and the intensity of extra electrostatic fields simulated by the density functional theory (DFT) method. (b) The net increase of the conversion of the condensation reaction between benzaldehyde and 1-pentanol was calculated from Table 1. The net increase means the conversion on Au/MZSM-5 deducts the conversion on its counterpart of MZSM-5 (M = H^+, Na^+, Ca^{2+}, or La^{3+}).

benzaldehyde by oxygen inevitably adsorbed on catalysts[42,43]. These results suggested the boosting effect of ENFE of Au-NPs held at different temperatures, and that the largest net increase of conversion was at 60°C. The reusability test shows that CaZSM-5 and Au/CaZSM-5 were very stable with above 95% retentions of original conversions after five runs (see SI, Section S7). Furthermore, the acetalization reaction between cyclohexanone and methanol showed similar cascade enhancement effect from visible light to zeoiltes (see SI, Section S8)[31,44].

In summary, the present study unravels a cascade enhancement effect from visible light to zeolite catalysts bridged via the ENFE of Au-NPs. The enhancement effect holds great potential in modifying the molecular polarities which affect the activity and electrostatic behavior of molecules and have broad applications in organic synthesis, ionic liquids, nanofiltration membranes, molecular electronics, and molecular self-assembly technology by means of non-covalent interactions[45–47]. This study should draw attention to a number of critical issues following this topic, considering more than 200 types of zeolites (IZA Framework Type Codes), and various plasmonic metal (or alloy) nanostructures together with their wide applications in sensing, solar panels, solar water splitting, photochemical synthesis, drug delivery, industrial processes of cracking and isomerization, and environmental remediation.

Methods

Preparation and ion-exchange of zeolites. All chemicals used for preparing zeolites were purchased from Sigma-Aldrich without further treatment. Silicalite-1 and ZSM-5 were synthesized by hydrothermal methods and were calcined at 550°C for 5 h with the step of increasing temperature being 5°C/min to remove organic templates. MZSM-5 (M = H^+, Na^+, Ca^{2+}, or La^{3+}) were obtained by standard ion-exchange procedures from the as-synthesized zeolites at 90°C for 3 h for each run, three times in total, under continuous stirring with 0.1 mol/L NH_4NO_3 aqueous solution to prepare HZSM-5, 0.1 mol/L sodium chloride (NaCl) aqueous solution to prepare NaZSM-5, 0.1 mol/L calcium chloride ($CaCl_2$) aqueous solution to prepare CaZSM-5, or 0.1 mol/L lanthanum(III) chloride ($LaCl_3$) aqueous solution to prepare LaZSM-5. After each run of ion-exchange, the samples were washed thoroughly with deionized water and then calcinations were conducted at 400°C for 3 hours.

Preparation of zeolites supported gold catalysts. Zeolites supported catalysts (Au/zeolite) catalysts were prepared by a reduction method. Typically, 1.25 g of zeolite fine powders were dispersed into 50 mL of 3.8×10^{-3} mol/L aqueous solution of chloroauric acid ($HAuCl_4$). Then 0.125 g of poly(vinyl alcohol) (PVA) was dispersed in 10 mL of deionized water; and the PVA solutions were added into the mixture of zeolite and $HAuCl_4$ solution under stirring for 0.5 h. To this suspension, 0.5 mL of 0.38 mol/L aqueous solution of tetrakis(hydroxymethyl) phosphonium chloride (THPC) was added drop by drop as the reducing agent, followed by adding 2.25 mL of 0.38 mol/L sodium hydroxide aqueous solution (NaOH). The mixture was stirred continuously for 2 h and aged statically for 24 h. Finally, the solid was washed with deionized water three times and ethanol once; and the obtained solids were dried at 60°C for 16 h. The dried solids were used directly as photocatalysts, denoted as Au/zeolite catalysts.

Characterization of catalysts. X-ray diffraction (XRD) patterns of the samples were detected on a Philips PANalytical X'Pert PRO diffractometer using Cu *Ka* radiation (λ = 1.5418 Å) at 40 kV and 40 mA. The diffraction data were collected from 5° to 75° with a resolution being 0.01° (2θ). UV/Visible (UV/Vis) spectra were recorded on a Cary 5000 UV/Vis-NIR Spectrophotometer in the wavelength range of 200–800 nm. The XPS data were recorded on an ESCALAB 250 spectrometer and Al *Ka* radiation was used as the X-ray source. The C1s peak at 284.8 eV was used as a reference for the calibration of the binding energy scale. Transmission electron microscopy (TEM) images were taken with a Philips CM200 Transmission electron microscope employing an accelerating voltage of 200 kV. The specimens were fine powders deposited onto a copper microgrid coated with a holey carbon film. The diffuse reflectance The FT-IR spectra were recorded on Nicolet Nexus 870 IR

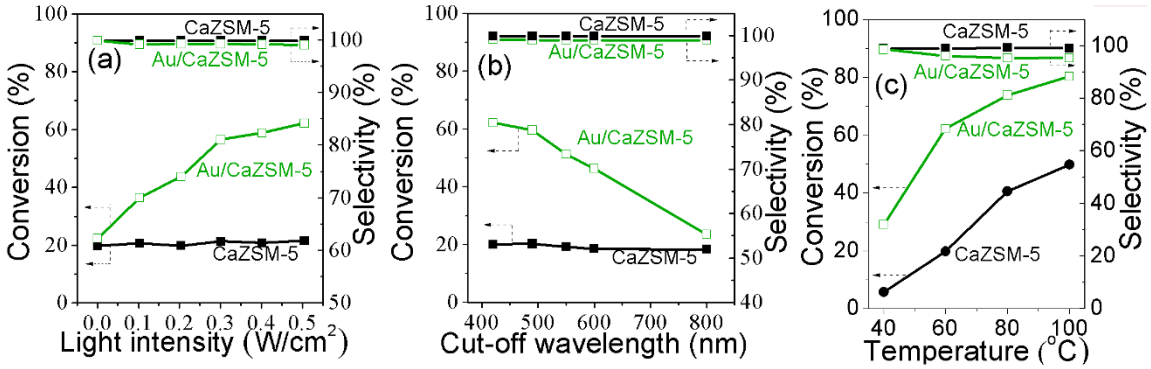

Figure 4 | The trend of conversion and selectivity of the acetalization between benzaldehyde and 1-pentanol varies as the function of light intensity (a), cut-off wavelength (b) (e.g. 420 nm means the light wavelength <420 nm is cut off, so the light used is from 420–800 nm), and the reaction temperature. (c) Reaction conditions: benzaldehyde (0.65 g), 1-pentanol (4.40 g), Au/ZSM-5 (0.05 g), atmosphere (argon), reaction temperature 60°C, and reaction time 6 h.

spectrophotometer equipped with a deuterated triglycine sulfate (DTGS) detector and a Diamond Attenuated Total Reflectance (ATR) Smart Accessory. 128 scans were collected for each measurement over the spectral range of 4000–650 cm^{-1} with a resolution of 4 cm^{-1}.

Catalytic test of Au/zeolites. All the raw chemicals were purchased from Sigma-Aldrich and used without further treatment. The batch reactions were conducted in a round-bottomed 50-mL transparent glass flask equipped with a sealed spigot and a magnetic stirrer. The reaction temperature was controlled by a portable air-conditioner in a sealed box. The flask was irradiated with a 500-Walt Halogen lamp, the UV light was removed by using a glass filter to cut off the light with the wavelength being shorter than 420 nm to avoid the possibility of direct inter-band transition in gold. The intensity of light source was from 0 (light off) to 0.505 W/cm^2. Aliquots (0.5 mL) were collected at given time intervals and filtrated through a Millipore filter (pore size 0.45 μm) to remove the catalyst particles. Control experiments were performed without light irradiation, maintaining the other conditions identical. The filtrates were analyzed by a Gas Chromatography (HP6890, HP-5 column) and GC-MS (6890-5793, HP-5MS column) was used to determine the components. Quantification of the products was obtained from the peak area ratios of the product and its corresponding reactant. The typical details of the chosen two reactions were as the following: the acetalization between benzaldehyde and 1-pentanol. Typically, 0.65 g of benzaldehyde was added into 4.40 g of 1-pentanol, and then 0.05 g catalyst was involved. The reaction temperature was controlled at 60°C. The acetalization of cyclohexanone with methanol produced dimethyl acetals. Typically, 1.0 g of cyclohexanone was mixed with 10 mL of methanol, and then 0.05 g of catalyst was added into this mixture. The reaction temperature was controlled at 40°C, and samples were withdrawn every 2 h.

1. El-Sayed, M. A. Some interesting properties of metals confined in time and nanometer space of different shapes. *Acc. Chem. Res.* **34**, 257–264 (2001).
2. Watanabe, K., Menzel, D., Nilius, N. & Freund, H.-J. Photochemistry on metal nanoparticles. *Chem. Rev.* **106**, 4301–4320 (2006).
3. Linic, S., Christopher, P. & Ingram, D. B. Plasmonic-metal nanostructures for efficient conversion of solar to chemical energy. *Nat. Mater.* **10**, 911–921 (2011).
4. Chen, X., Zhu, H. Y., Zhao, J. C., Zheng, Z. F. & Gao, X. P. Visible-light-driven oxidation of organic contaminants in air with gold nanoparticle catalysts on oxide supports. *Angew. Chem. Int. Ed.* **47**, 1–5 (2008).
5. Zhang, X. G., Ke, X. B. & Zhu, H. Y. Zeolite-supported gold nanoparticles for selective photooxidation of aromatic alcohols under visible-light irradiation. *Chem. Euro. J.* **18**, 8048–8056 (2012).
6. Zhu, H. Y., Ke, X. B., Yang, X. Z., Sarina, S. & Liu, H. W. Reduction of nitroaromatic compounds on supported gold nanoparticles by visible and ultraviolet light. *Angew. Chem. Int. Ed.* **49**, 9657–9661 (2010).
7. Ke, X. B. *et al.* Tuning the reduction power of supported gold nanoparticle photocatalysts for selective reductions by manipulating the wavelength of visible light irradiation. *Chem. Commun.* **48**, 3509–3511 (2012).
8. Christopher, P., Xin, H. L. & Linic, S. Visible-light-enhanced catalytic oxidation reactions on plasmonic silver nanostructures. *Nat. Chem.* **3**, 467–472 (2011).
9. Marimuthu, A., Zhang, J. W. & Linic, S. Tuning selectivity in propylene epoxidation by plasmon mediated photo-switching of Cu oxidation state. *Science* **29**, 1590–1593 (2013).
10. Wang, F., Li, C. H., Chen, H. J., Jiang, R. B., Sun, L.-D., Li, Q., Wang, J. F., Yu, J. C. & Yan, C.-H. Plasmonic harvesting of light energy for Suzuki coupling reactions. *J. Am. Chem. Soc.* **135**, 5588–5601 (2013).
11. Sarina, S. *et al.* Enhancing catalytic performance of palladium in gold and palladium alloy nanoparticles for organic synthesis reactions through visible light irradiation at ambient temperatures. *J. Am. Chem. Soc.* **135**, 5793–5801 (2013).
12. Xiao, M. D. *et al.* Plasmon-enhanced chemical reactions. *J. Mater. Chem. A* **1**, 5790–5805 (2013).
13. Nie, S. & Emory, S. R. Probing single molecules and single nanaoparticles by surface-enhanced Raman scattering. *Science* **275**, 1102–1106 (1997).
14. Xu, X. B., Kim, K., Li, H. F. & Fan, D. L. Ordered arrays of Raman nanosensors for ultrasensitive and location predictable biochemical detection. *Adv. Mater.* **24**, 5457–5463 (2012).
15. Tang, L. *et al.* Nanometer-scale germanium photodetector enhanced by a near-infrared dipole antenna. *Nat. Photonics* **2**, 226–229 (2008).
16. Liu, W. J. *et al.* Gold nanorod@chiral mesoporous silica core−shell nanoparticles with unique optical properties. *J. Am. Chem. Soc.* **135**, 9659–9664 (2013).
17. Challener, W. A. *et al.* Heat-assisted magenetic recording by a near field transducer with efficient optical energy transfer. *Nat. Photonics*, **3**, 220–224 (2009).
18. Maier, S. A. *et al.* Local detection of electromagnetic energy transport below the diffraction limit in metal nanoparticle plasmon waveguides. *Nat. Mater.* **2**, 229–232 (2003).
19. Shelby, R. A., Smith, D. R. & Schultz, S. Experimental verification of a negative index of refraction. *Science* **292**, 77–79 (2001).
20. Gan, Q. Q., Bartoli, F. J. & Kafafi, Z. H. Plasmonic-enhanced organic photovoltaics: breaking the 10% efficiency barrier. *Adv. Mater.* **25**, 2385–2396 (2013).
21. Gu, M. *et al.* Nanoplasmonics: a frontier of photovoltaic solar cells. *Nanophotonics* **1**, 235–248 (2012).
22. Awazu, K. *et al.* A plasmonic photocatalyst consisting of silver nanoparticles embedded in titanium dioxide. *J. Am. Chem. Soc.* **130**, 1676–1680 (2008).
23. Bordiga, S., Garrone, E., Lamberti, C. & Zecchina, A. Low-temperature Fourier transform infrared study of the interaction of CO with cations in alkali-metal exchanged ZSM-5 zeolites. *J. Chem. Soc. Fraday Trans.* **90**, 3367–3372 (1994).
24. Xiang, Y., Larsen, S. C. & Grassian, V. H. Photooxidation of 1-alkenes in zeolites: a study of the factors that influence product selectivity and formation. *J. Am. Chem. Soc.* **121**, 5063–5072 (1999).
25. Tsutsumi, K. &Takahashi, H. A study of the nature of active sites on zeolites by the measurement of heat of immersion. II. Effects of silica/alumina ratio to electrostatic-field strength of calcium-exchanged zeolites. *J. Phys. Chem.* **76**, 110–115 (1972).
26. Sun, H., Blatter, F. & Frei, H. Selective oxidation of toluene to benzaldehyde by O_2 with visible light in Barium(2+)- and Calcium(2+)-exchanged zeolite Y. *J. Am. Chem. Soc.* **116**, 7951–7952 (1994).
27. Sun, H., Blatter, F. & Frei, H. Cyclohexanone from cyclohexane and O_2 in a zeolite under visible light with complete selectivity. *J. Am. Chem. Soc.* **118**, 6873–6879 (1996).
28. Blatter, F. & Frei, H. Selective photooxidation of small alkenes by O_2 with red light in zeolite Y. *J. Am. Chem. Soc.* **116**, 1812–1820 (1994).
29. Frei, H. Selective hydrocarbon oxidation in zeolites. *Science* **313**, 309–310 (2006).
30. Liu, F. J. *et al.* ZSM-5 zeolite single crystals with *b*-axis-aligned mesoporous channels as an efficient catalyst for conversion of bulky organic molecules. *J. Am, Chem. Soc.* **134**, 4557–4560 (2012).
31. Iwamoto, M., Tanaka, Y., Sawamura, N. & Namba, S. Remarkable effect of pore size on the catalytic activity of mesoporous silica for the acetalization of cyclohexanone with methanol. *J. Am. Chem. Soc.* **125**, 13032–13033 (2003).
32. Kim, J. H., Čorič, I., Vellalath, S. & List, B. The catalytic asymmetric acetalization. *Angew. Chem. Int. Ed.* **52**, 4474–4477 (2013).
33. Ogura, M. *et al.* Alkali-treatment technique–new method for modification of structural and acid-catalytic properties of ZSM-5 zeolites. *Appl. Catal. A* **219**, 33–43 (2001).
34. Xu, J., Mojet, B. L., van Ommen, J. G. & Lefferts, L. Effect of Ca^{2+} position in zeolite Y on selective oxidation of propane at room temperature. *J. Phys. Chem. B* **108**, 15728–15734 (2004).
35. Khatri, O. M., Murase, K. & Sugimura, H. Structural organization of gold nanoparticles onto the ITO surface and its optical properties as a function of ensemble size. *Langmuir* **24**, 3787–3793 (2008).
36. Jin, F. & Li, Y. D. A FTIR and TPD examination of the distributive properties of acid sites on ZSM-5 zeolite with pyridine as a probe molecule. *Catal. Today* **145**, 101–107 (2009).
37. Cho, H., Park, H., Russell, T. P. & Park, S. Precise placements of metal nanoparticles from reversible block copolymer nanostructures. *J. Mater. Chem.* **20**, 5047–5051 (2010).
38. Dunne, J. A., Rao, M., Sircar, S., Gorte, R. J. & Myers, A. L. Calorimetric heats of adsorption and adsorption isotherms. 2. O_2, N_2, Ar, CO_2, CH_4, C_2H_6, and SF_6 on NaX, H-ZSM-5, and Na-ZSM-5 zeolites. *Langmuir* **12**, 5896–5904 (1996).
39. Bär, T., Visart de Bocarmé, T., Nieuwenhuys, B. E. & Kruse, N. CO oxidation on gold surfaces studied on the atomic scale. *Catal. Lett.* **74**, 127–131 (2001).
40. Wustholz, K. L. *et al.* Structure-activity relationships in gold nanoparticle dimers and trimers for surface-enhanced raman spectroscopy. *J. Am. Chem. Soc.* **132**, 10903–10910 (2010).
41. Large, N., Abb, M., Aizpurua, J. & Muskens, O. L. Plasmonic near-electric field enhancement effects in ultrafast photoelectron emission: correlated spatial and laser polarization microscopy studies of individual Ag nanocubes. *Nano Lett.* **10**, 1741–1746 (2010).
42. Bulanin, K. M. & Lobo, R. F. Low-temperature adsorption of N_2, O_2, and D_2 on LiX, NaX, and NaLiX zeolites studied by FT-IR spectroscopy. *J. Phys. Chem. B* **104**, 1269–1276 (2000).
43. Xu, J., Mojet, B. L., van Ommen, J. G. & Lefferts, L. Formation of $M^{2+}(O_2)(C_3H_8)$ species in alkaline-earth-exchanged Y zeolite during propane selective oxidation. *J. Phys. Chem. B* **109**, 18361–18368 (2005).
44. Shetti, V. N., Kim, J., Srivastava, R., Choi, M. & Ryoo, R. Assessment of the mesopore wall catalytic activities of MFI zeolite with mesoporous/microporous hierarchical structures. *J. Catal.* **254**, 296–303 (2008).
45. Van der Bruggen, B., Schaep, J., Wilms, D. & Vandecasteele, C. Influence of molecular size, polarity and charge on the retention of organic molecules by nanofiltration. *J. Membrane Sci.* **156**, 29–41 (1999).
46. Lewis, P. A., Inman, C. E., Maya, F., Tour, J. M., Hutchison, J. E. & Weiss, P. S. Molecular engineering of the polarity and interactions of molecular electronic switches. *J. Am. Chem. Soc.* **127**, 17421–17426 (2005).
47. Singh, A. S. & Sun, S.-S. Dynamic self-assembly of molecular capsules via solvent polarity controlled reversible binding of nitrate anions with C_3 symmetric tripodal receptors. *Chem. Commun.* **47**, 8563–8565 (2011).

Acknowledgments

This research is supported by the Australian Research Council (ARC) and X. Ke is indebted to QUT and the Queensland State Government for a Smart Futures Fellowship.

Author contributions

X.Z. conducted the experiments, sample characterization and data analysis. X.K. designed the experiments and prepared parts of the materials. A.D. conducted DFT calculations and helped revise the manuscript. H.Z. proposed the study and contributed important suggestions. The manuscript was written by X.Z. and X.K.

Additional information

Supplementary information accompanies this paper at http://www.nature.com/scientificreports

Competing financial interests: The authors declare no competing financial interests.

How to cite this article: Zhang, X.G., Ke, X.B., Du, A.J. & Zhu, H.Y. Plasmonic nanostructures to enhance catalytic performance of zeolites under visible light. *Sci. Rep.* **4**, 3805; DOI:10.1038/srep03805 (2014).